JTTEE5 25:587–594
DOI: 10.1007/s11666-016-0381-0
1059-9630/$19.00 © ASM International

Hot Corrosion Behavior of Low-Pressure Cold-Sprayed CoNiCrAlY Coatings

L.W. Zhang, X.J. Ning, L. Lu, Q.S. Wang, and L. Wang

(Submitted November 10, 2015; in revised form December 18, 2015)

CoNiCrAlY coatings were deposited by low-pressure cold spraying and pre-oxidized in a vacuum environment, and its hot corrosion behavior in pure Na_2SO_4 and 75 wt.% Na_2SO_4 + 25 wt.% NaCl salts was investigated. The pre-oxidation treatment resulted in the formation of a dense and continuous α-Al_2O_3 scale on the coating surface. After being corroded for 150 h at 900 °C, the pre-oxidized coating exhibited better corrosion resistance to both salts than the as-sprayed coating. The presence of pre-formed Al_2O_3 scale reduced the consumption rate of aluminum, by delaying the formation of internal oxides and sulfides and promoting the formation of a denser and more adherent Al_2O_3 scale. Moreover, we investigated the corrosion mechanism of cold-sprayed CoNiCrAlY coatings in the two salts and discussed the effect of the pre-oxidation treatment.

Keywords cold spray, hot corrosion, MCrAlY coating, oxidation, pre-oxidation

1. Introduction

The hot components of gas turbines operating at high temperature under environments containing sodium, sulfur, and vanadium will suffer hot corrosion, during which the consumption of the material can proceed at an unpredictably rapid rate (Ref 1). MCrAlY (M = Ni and/or Co) coatings are commonly used as overlays to extend the service life of hot components in gas turbines exposed to oxygen at high temperature, combined in many cases with a corrosive environment (Ref 2-4). The control of oxide scale growth and structure has attracted considerable interest, because oxide scales such as Al_2O_3 and Cr_2O_3 play an important role in protecting the base alloy from hot corrosion (Ref 5).

The service life of MCrAlY coatings in a corrosive environment is determined by the stability of the Al_2O_3/Cr_2O_3 scale formed on their surface. However, the dissolution of Al_2O_3/Cr_2O_3 scales due to reaction with salts (regardless of the reaction mechanism involved) is inevitable, especially when the coating is exposed directly to molten salt. Therefore, another effective way to prolong the life of MCrAlY coatings is to form the protective scale prior to hot corrosion. It has been reported that a pre-oxidation treatment is beneficial to the high-temperature oxidation resistance of high-velocity oxygen fuel (HVOF)-sprayed CoNiCrAlY coatings, as well as to the salt fog corrosion resistance of arc ion-plated NiCoCrAlYBSi coatings (Ref 6, 7). Therefore, it is essential to investigate the effect of a pre-oxidation treatment on the hot corrosion behavior of MCrAlY coatings.

In recent years, cold spraying has attracted increasing interest as a route for depositing MCrAlY coating with remarkably low oxygen content and porosity, thanks to its low deposition temperature and severe plastic deformation during the deposition process (Ref 8, 9). Recent research pointed out that the properties of cold-sprayed MCrAlY coatings favor of the formation of a uniform and dense α-Al_2O_3 scale, which imparts excellent high-temperature oxidation resistance to the coating (Ref 10-12). However, relatively little research has been conducted on the hot corrosion behavior of cold-sprayed MCrAlY coatings.

In this study, a CoNiCrAlY coating was deposited by low-pressure cold spraying and then pre-oxidized in a vacuum environment. The hot corrosion behavior of the cold-sprayed coating in molten Na_2SO_4 and 75 wt.% Na_2SO_4 + 25 wt.% NaCl salts was then investigated, and the hot corrosion mechanism of the coating was also discussed.

2. Experimental Procedures

2.1 Materials and Coating Preparation

A commercial CoNiCrAlY feedstock powder [with nominal composition Co-68.5Ni-32Cr-21Al-8Y-0.5 (wt.%)] was used to deposit a coating by a low-pressure cold spraying system (KM-CDS 3.2, Inovati Ltd. Co., USA). The powder exhibited a spherical morphology and an average size of 11 μm. A nickel-based superalloy GH4049 [with nominal composition of Ni-15Co-10Cr-5.5W-4Al-1.7Ti (wt.%)] was used as substrate. Helium gas with an inlet pressure of 0.62 MPa and a temperature of

L.W. Zhang and **L. Lu**, Jiangxi Key Laboratory for Advanced Copper and Tungsten Materials, Jiangxi Academy of Sciences, Nanchang 330029, China; and **X.J. Ning**, **Q.S. Wang**, and **L. Wang**, National Key Laboratory of Science and Technology on Materials Under Shock and Impact, Beijing Institute of Technology, Beijing 100081, China. Contact e-mail: nxj@bit.edu.cn.

520 °C was used as the propellant and feeding gas. The nozzle was set to a standoff distance of 10 mm from the substrate and with transverse speed of 70 mm/s.

2.2 Heat Treatment and Hot Corrosion Test

After deposition, some samples were heated to 1050 °C at a rate of 5 °C/min, and held at that temperature for 4 h in a vacuum furnace at a pressure of 10^{-3} Pa. The hot corrosion behavior was assessed by salt-coating test at high temperature. To enhance the adhesion of the salt, the as-sprayed and pre-oxidized samples were heated to 150 °C. Subsequently, aqueous salt solutions of Na_2SO_4 and 75 wt.% $Na_2SO_4 + 25$ wt.% NaCl were sprayed onto the coating surface. The weight of the salt after drying was kept to 3-4 mg/cm^2. Finally, the coated samples were placed in a high-temperature furnace at 900 °C to perform the corrosion test. During the test, all samples were removed from the furnace every 10 h and allowed to cool down to room temperature. Then, the samples were cleaned with boiling distilled water to remove residual salt and dried for the new salt film preparation.

2.3 Characterization

The oxygen contents of the feedstock powder and the as-sprayed coating were examined by an oxygen analyzer (TC-436, LECO, USA). The microstructure of the coatings and corrosion scale was characterized by a scanning electron microscope (SEM) equipped with an energy dispersion spectrometer (EDS). The crystalline phases present in powder, coating, and corrosion scale were identified by x-ray diffraction (XRD). To prevent spallation of the corrosion scale during the preparation of cross-sectional samples, the sample surfaces were plated with Ni using an electroless process. The composition of the corrosion scale after vacuum heat treatment was determined using a laser fluorescence spectrophotometer (HJY LabRAM Aramis). Based on the cross-sectional SEM images, the area of the Al-depletion zone and the length of the corrosion scale/coating interface were analyzed by a commercial software (Image-Pro Plus 6.0). The area of the Al-depletion zone was measured by drawing a polygon along the corrosion scale/coating and Al-depletion/Al-rich zone interfaces. More than 30 random images were analyzed in order to obtain the mean area and length values for each sample, and the average thickness of Al-depletion zone was then defined as

$$\delta eq = \frac{\sum S}{\sum L}, \qquad \text{(Eq 1)}$$

where S and L represent the area of the Al-depletion zone and the length of the corrosion scale/coating interface.

3. Results and Discussion

3.1 Structure of the Coatings Prior to Hot Corrosion

Figure 1 shows the cross-sectional morphology of as-sprayed and pre-oxidized coatings. The image was obtained in back-scattered electron (BSE) mode. Despite some irregularity in the surface layer, the as-sprayed coating exhibited a considerably dense structure, which can be attributed to the peening effect of the particles impacting on the deposited surface. This effectively promoted an increase in the density of the deposited coating, as reported in other cold-spray processing (Ref 13). Moreover, the oxide content of the as-sprayed coating was 0.12 wt.%, compared with 0.08 wt.% for the feedstock powder. Since the temperature of CoNiCrAlY particles is much lower than the melting point of the powder material, only minor oxidation occurs during the deposition process, which is one of the characteristic features of cold-sprayed coatings. After heat treatment, the irregularity was eliminated and a thin oxide scale was formed on the coating surface (Fig. 1b). Further analysis of fluorescence spectra

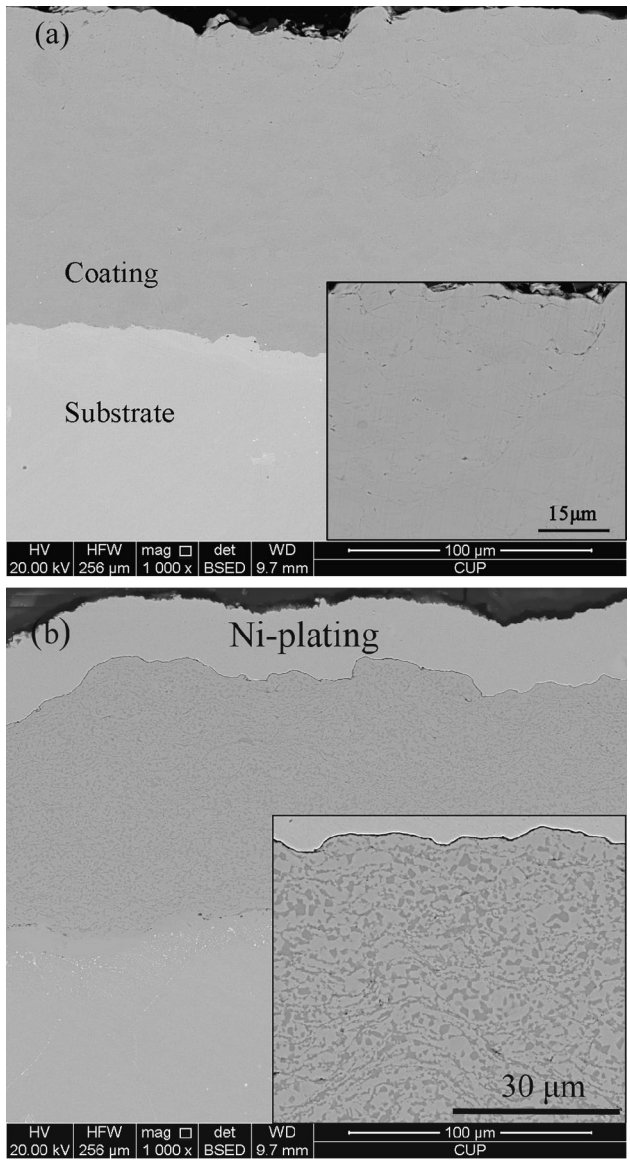

Fig. 1 Cross-sectional BSE images of as-sprayed coating (a) and pre-oxidized coating (b)

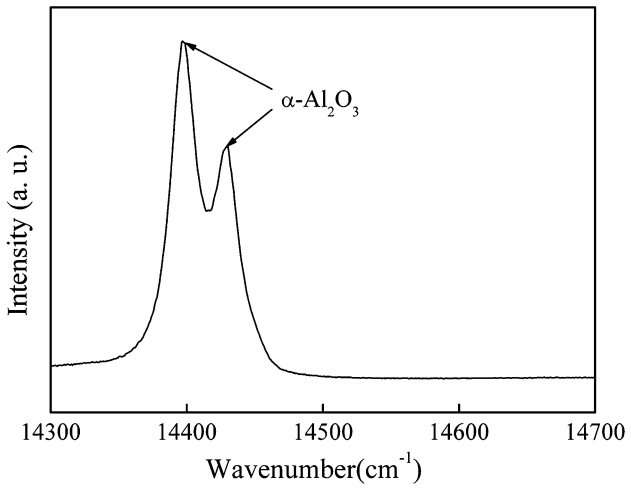

Fig. 2 Fluorescence spectra result of surface of the pre-oxidized coating

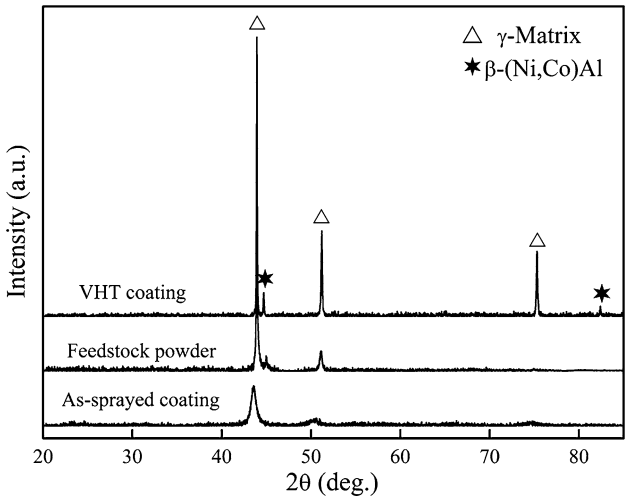

Fig. 3 XRD patterns of as-received powder, as-sprayed coating, pre-oxidized coating

indicated that the oxide scale consists of pure α-Al_2O_3 (Fig. 2). No obvious Al-depletion zone can be observed underneath the Al_2O_3 scale, implying that no over-consumption of Al occurred during the pre-oxidation heat treatment. The formation of a dense and aluminum-saving α-Al_2O_3 scale is crucial for the industrial application of pre-oxidation treatment approaches. It has been reported that the oxide scale of an HVOF CoNiCrAlY coating pre-oxidized at 1080 °C and $<10^{-3}$ Pa for 4 h consisted of α-Al_2O_3 and spinel oxides (Ref 6). In the present case, an oxide scale consisting of only pure α-Al_2O_3 was obtained. This contributed to the formation of a structure with a high density and low oxygen content.

Figure 3 shows the XRD patterns of CoNiCrAlY feedstock powder, as-sprayed coating, and pre-oxidized coating. An obvious broadening in the peaks of the γ-matrix phase were observed in the 2θ range of 40-50° for the as-sprayed coating, which can be attributed to grain refinement and/or micro-stress induced from severe plastic deformation of the deposited particles. Moreover, the peaks associated with the β-(Ni,Co)Al phase were almost undetectable in the as-sprayed coating, based on both the cross-sectional structure (Fig. 1a) and XRD patterns (Fig. 3). Taking into account the fact that the particle experienced quite low temperatures during the coating deposition, it can be hypothesized that the β phase was dispersed and dissolved into the γ-matrix phase due to the severe plastic deformation, which is consistent with the phenomenon reported in the literature (Ref 14). After vacuum heat treatment, the width of the diffraction peaks associated with the γ phase became much narrower and the coating showed a typical β/γ dual-phase structure. This result indicates that vacuum heat treatment provides the driving force for crystallization and grain growth of the coating.

3.2 Hot Corrosion Tests

Figure 4 shows the XRD patterns of the surface corrosion scale after 150 h of corrosion. Following corrosion

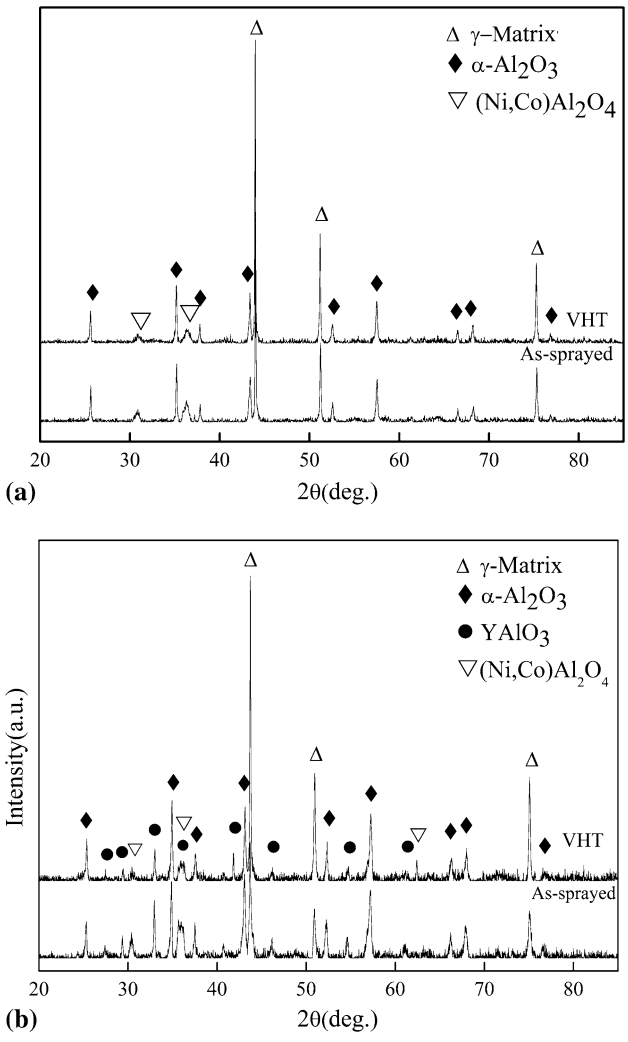

Fig. 4 XRD patterns of coatings after 150 h corrosion in Na_2SO4 (a) and 75 wt.% Na_2SO_4 + 25 wt.% NaCl (b)

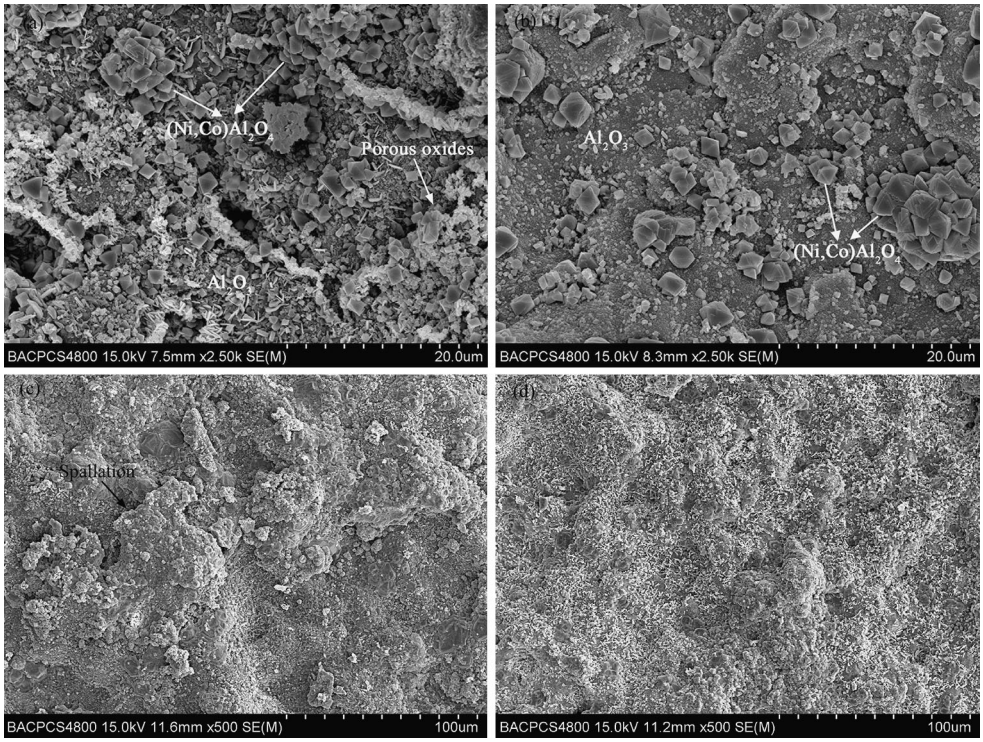

Fig. 5 Surface SEM images of as-sprayed coating (a, c) and pre-oxidized coating (b, d) after 150 h corrosion (a, b: corrosion in Na_2SO_4; c, d: corrosion in 75 wt.% Na_2SO_4 + 25 wt.% NaCl)

in pure Na_2SO_4, the corrosion scales on the as-sprayed and pre-oxidized coatings consisted mainly of α-Al_2O_3, with a minor $(Ni,Co)Al_2O_4$ spinel component. On the other hand, upon corrosion in the mixture salt, relatively higher contents of $(Ni,Co)Al_2O_4$ spinel and $YAlO_3$ were formed besides α-Al_2O_3 on the surface of both coatings. However, α-Al_2O_3 still represented the main corrosion scale. The typical surface morphologies of the coatings after 150 h corrosion are shown in Fig. 5. Some porous oxides were observed on the as-sprayed coating surface, which means that severe hot corrosion occurred for the as-sprayed coatings after 150 h corrosion in pure Na_2SO_4. However, the pre-oxidized coating surface was very smooth and the corrosion scales consisted of α-Al_2O_3 and $(Ni,Co)Al_2O_4$. After corrosion in the mixture salt, local spallation of the corrosion scale can be observed for the as-sprayed coating. By contrast, the pre-oxidized coating exhibited uniform and crack-free surfaces. It can thus be concluded that the corrosion scale generated on the basis of the preformed α-Al_2O_3 scale shows better spalling resistance than that formed by direct corrosion of the mixed salt.

Figure 6 shows the cross-sectional BSE images of the CoNiCrAlY coatings after corrosion in pure Na_2SO_4 for 100 and 150 h. After corrosion for 100 h, a dense and continuous α-Al_2O_3 scale was formed on the as-sprayed and pre-oxidized coatings. In the case of the as-sprayed coating, a few internal oxides and chromium sulfides can be found underneath the corrosion scale. As corrosion advanced, the corrosion scales formed on both coatings were still composed of α-Al_2O_3, while a small amount of internal oxide and chromium sulfide formed underneath the α-Al_2O_3 layer. The as-sprayed and pre-oxidized coatings both suffered slight corrosion after 150 h in pure Na_2SO_4, with Al-depletion zone depths of approximately 9.6 and 8.8 μm, respectively.

Figure 7 shows the cross-sectional BSE images of the CoNiCrAlY coatings after corrosion in 75 wt.% Na_2SO_4 + 25 wt.% NaCl for 20 and 150 h. After 20 h, the corrosion scale formed on the as-sprayed coating consisted mainly of α-Al_2O_3, with minor spinel and $YAlO_3$ components (Fig. 7a), whereas the pre-oxidized coating led to a rather uniform and continuous pure α-Al_2O_3 scale (Fig. 7b). At the same time, internal oxides and chromium sulfides were observed within the as-sprayed coating. It should be noticed that in this case no internal corrosion products were observed within the pre-oxidized coating. After corrosion for 150 h, a much thicker but still continuous Al_2O_3 scale was formed on the pre-oxidized coating (Fig. 7d). Lamellar cracks were found in the corrosion scale of the as-sprayed coating (Fig. 7c). Furthermore, a large amount of internal oxides and chromium sulfides could be observed for both coatings. Compared with the microstructure of coatings corroded in pure Na_2SO_4 (Fig. 6c, d), the Al-depletion zone depth of the as-sprayed coating was notably extended from less than 50 μm to approximately 76 μm. In the case of the pre-oxidized coating, the Al-depletion zone depth was relatively uniform, with a depth of approximately 27.5 μm.

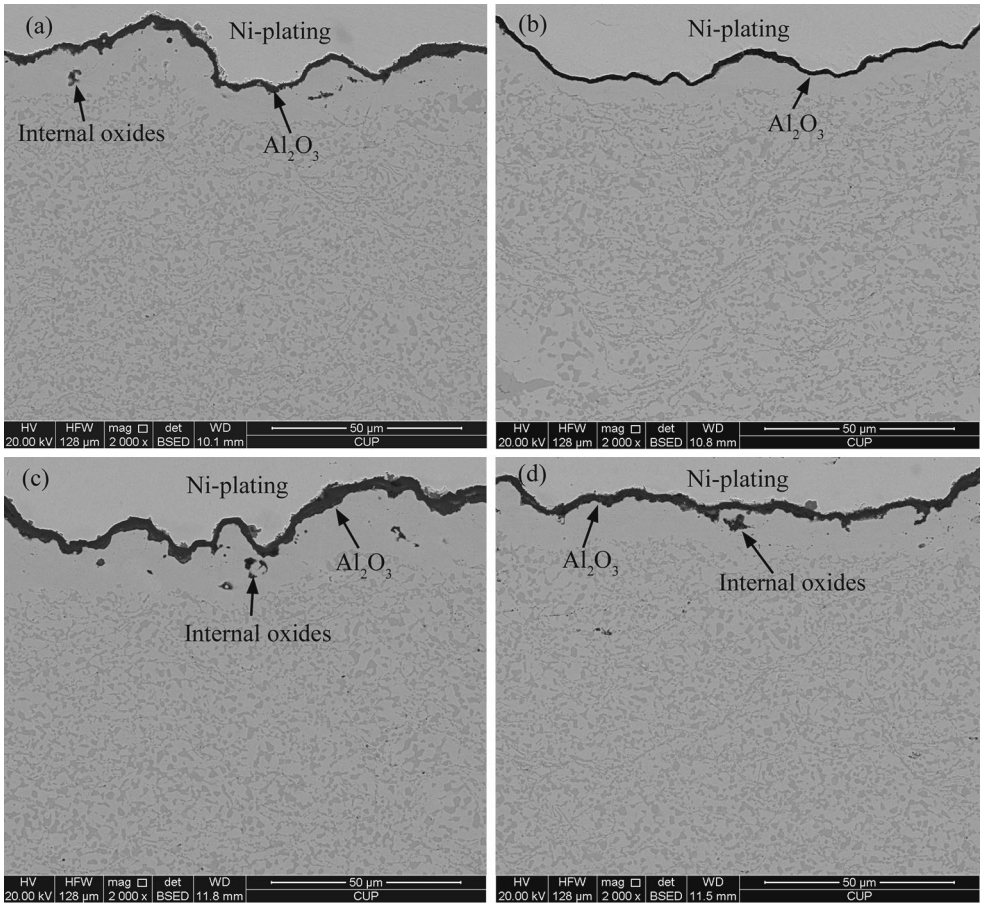

Fig. 6 Cross-sectional BSE images of as-sprayed (a, c) and pre-oxidized (b, d) coatings after corrosion in pure Na_2SO_4 (a, b: corrosion for 100 h; c, d: corrosion for 150 h)

The difference in the uniformity of the Al-depletion zone depth can be attributed to the cracks formed in the corrosion scale of the as-sprayed coating. Oxygen, sulfur and chlorine can enter into coating through cracks directly, not just through grain boundary and voids in the Al_2O_3 scale. Significant amounts of β-(Ni,Co)Al phase were still present underneath the Al-depletion zone for as-sprayed coatings, which is expected to provide a sufficient supply of Al to repair protective Al_2O_3 scale rapidly. Comparatively, the pre-oxidized coating showed high resistance to hot corrosion. Figure 8 shows the change in thickness of the Al-depletion zone as a function of corroding time for the CoNiCrAlY coatings in mixture salt. The pre-oxidized coating showed lower Al consumption rate than the as-sprayed coating, which can be attributed to the fact that internal oxidation and sulfidation were delayed by the pre-oxidation treatment, as shown in Fig. 7(c) and (d). As can be also seen in Fig. 8, the growth of the Al-depletion of zone followed an almost linear (rather than parabolic) trend. This indicates that the growth of Al_2O_3 scale was not controlled by aluminum and oxygen along the oxide grain boundary, as usually occurs for high-temperature oxidation processes.

4. Hot Corrosion Mechanisms for Cold-Sprayed CoNiCrAlY Coating

Previous studies indicate that the Na_2SO_4 melt is stable under a rather wide range of oxygen pressures, from about 10^{-7} to 10^5 Pa (Ref 15, 16). The following equilibrium exists in fused Na_2SO_4:

$$SO_4^{2-} = O^{2-} + SO_3 = O^{2-} + SO_2 + \frac{1}{2}O_2 \qquad \text{(Eq 2)}$$

The activity of Na_2O and SO_3 determine the melt basicity and acidity, respectively. As the temperature exceeds 827 °C, a fused Na_2SO_4 film can be formed on the as-sprayed coating surface, and simultaneously an oxidation similar to the ambient oxidation will take place. It should be noted that the metal reacts with SO_3 in Na_2SO_4 rather than with oxygen from the atmosphere, due to the quite low solubility of oxygen in the melt (Ref 17-20). Therefore, the oxygen potential at the salt/metal interface will decrease while the sulfur potential and activity of O^{2-} will increase, as indicated by Eq 2. The coating may exhibit a so called ''latent'' stage until the sulfur potential and activity of O^{2-} increase to a level high enough for basic

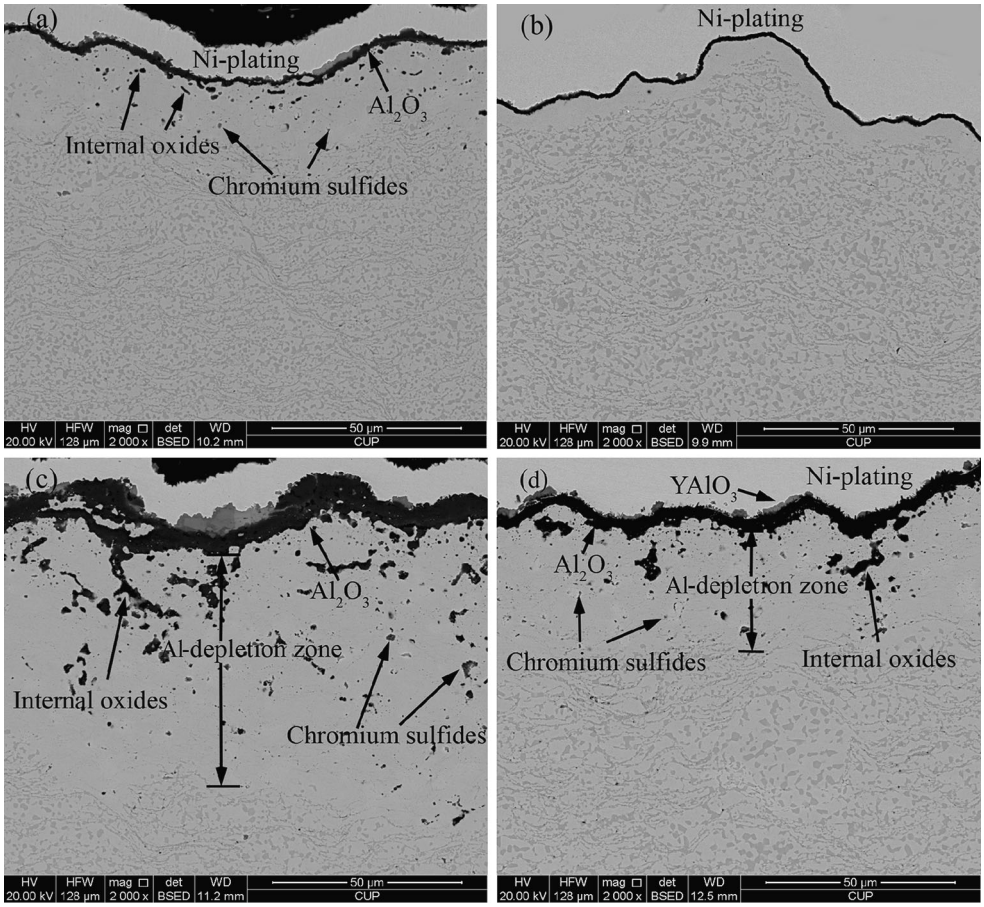

Fig. 7 Cross-sectional BSE images of as-sprayed (a, c) and pre-oxidized (b, d) coatings after corrosion in 75 wt.% Na_2SO_4 + 25 wt.% NaCl (a, b: corrosion for 20 h; c, d: corrosion for 150 h)

fluxing, as reported for most alloys under Na_2SO_4 melt hot corrosion (Ref 18). The results of this study suggest that the length of the latent stage exceeds 50 h for the as-sprayed CoNiCrAlY coating, after which the appearance of internal oxide and sulfides can be observed (Fig. 6a). This can be attributed to the significantly dense structure of coatings, as well as to the single γ-matrix phase with refined grains, which provide more grain boundaries for aluminum diffusion in the initial corrosion stage. For the pre-oxidized coating, the preformed continuous Al_2O_3 scale acted as a natural barrier to prevent direct contact between molten salt and coating. The initial stage consists in the inward diffusion of Na_2SO_4 through the grain boundary and voids in the corrosion scale. It can be suggested that the selective oxidation of aluminum by diffused SO_4^{2-} ions resulted in a lower sulfur potential and basicity at the salt/oxide interface, compared with the case of as-sprayed coating at this stage. As a result, the pre-oxidized coating corroded for 100 h presents a slighter basic fluxing of oxide, without internal oxides and sulfides (Fig. 6b). In other words, the latent stage of hot corrosion for CoNiCrAlY coating was extended by the pre-oxidation treatment.

With the increased activity of O^{2-} in the molten salt, the basic fluxing of Al_2O_3 will occur as indicated in Eq 3:

$$Al_2O_3 + O^{2-} = 2AlO_2^- \quad \text{(Eq 3)}$$

The coating then experiences a competition between the repeated basic fluxing of Al_2O_3 scale and the formation of oxide scale. Finally, the higher growth rate results in a net increase in the oxide scale thickness during the further hot corrosion stage, as demonstrated in Fig. 6(c) and (d).

When NaCl was added into the Na_2SO_4 melt, the corrosion became more severe and complex compared with pure Na_2SO_4. This conclusion can be drawn from the formation time of internal corrosion products and the corrosion depth of both coatings after corrosion for 150 h, as shown in Fig. 6 and 7. In the initial stage, although the preformed Al_2O_3 scale on the surface of the pre-oxidized coating can effectively prevent the direct contact between coating and fused salts, the chlorine ions can still transform the Al_2O_3 scale through the grain boundaries as well as the defects generated by basic fluxing of Na_2SO_4 to react with the metal underneath the Al_2O_3 scale. It is believed that NaCl-induced hot corrosion is initiated by the reaction of metal, oxygen, and NaCl to form metal

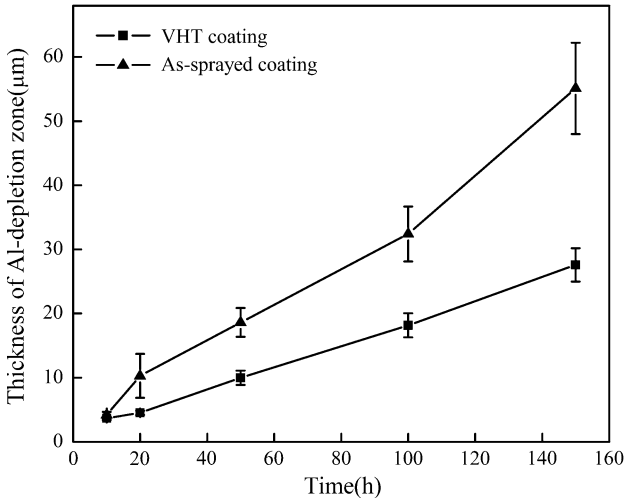

Fig. 8 Changes of Al-depletion zone thickness against time of hot corrosion

Table 1 Thermodynamic data of relevant metal chlorides at 900 °C (Ref 23)

Compound	ΔG^0_{1173}, kJ/mol
$AlCl_3(g)$	−522.414
$CrCl_3(s)$	−293.318
$CoCl_2(g)$	−162.107
$NiCl_2(s)$	−133.672

oxide and release chlorine (Ref 21, 22). Table 1 lists thermodynamic data of several metal chlorides at 900 °C According to these data, among the elements present in the CoNiCrAlY coating, Al and Cr are the first to form $AlCl_3$ and $CrCl_3$ by the chlorine-driving reaction. Furthermore, the $AlCl_3$ vapor may diffuse more rapidly than the $CrCl_3$ one, due to the much higher vapor pressure of $AlCl_3$ (Ref 24). As $AlCl_3$ evaporates to the area with higher concentration of oxygen, the onset of oxidation occurs to form internal oxides (such as Al_2O_3 in this study) and release chlorine, as described by Eq 4:

$$2AlCl_3(g) + \frac{3}{2}O_2(g) = Al_2O_3(s) + 3Cl_2(g). \quad \text{(Eq 4)}$$

Based on the above process, the coating will suffer successive corrosion as Cl_2 penetrates into the coating again. As a result, the Cl^- ions present will accelerate the coating degradation by consumption of beneficial Al.

When the as-sprayed CoNiCrAlY coating is exposed directly to fused mixed salt, the consumption of aluminum derives from its selective oxidation to form Al_2O_3 scales and internal oxides with the participation of sodium chloride, as discussed above. The aluminum consumption rate in the initial stage is much higher than that for the pre-oxidized coating, which results in a thicker depletion zone, as shown in Fig. 8. In the subsequent hot corrosion stage, the contact between metal and sulfur or chlorine ions for both coatings was dominated by the diffusion

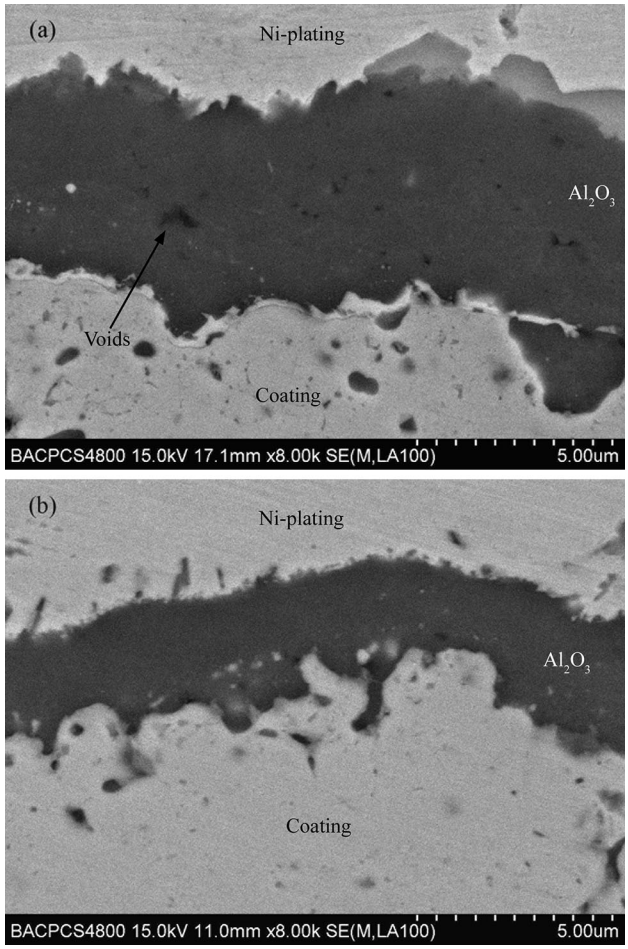

Fig. 9 Cross-sectional structure of corrosion scale of as-sprayed (a) and pre-oxidized (b) coatings after 150 h corrosion

through grain boundary and voids in the Al_2O_3 scale. The denser structure with fewer voids of the Al_2O_3 scale formed on the pre-oxidized coating can provide a better barrier to the diffusion of sulfur and chlorine ions, as shown in Fig. 9. Hence, the pre-oxidized coating showed better resistance to hot corrosion compared with as-sprayed coating. The photograph shown in Fig. 9 was obtained in the secondary electron mode, while those in Fig. 7(c) and (d) were obtained in BSE mode.

In short, on the basis of the above results and discussion, it can be concluded that the pre-oxidation treatment not only delayed the formation of internal oxides and sulfides, but also led to the formation of a denser and more adherent Al_2O_3 scale.

5. Conclusions

(1) The cold-sprayed CoNiCrAlY coating exhibited a dense and crack-free structure consisting of a single γ-matrix phase. A uniform and continuous single α-Al_2O_3 layer can be formed by pre-oxidation treatment in a vacuum environment.

(2) Compared to as-sprayed coating, the pre-oxidized coating showed better corrosion resistance to both pure Na_2SO_4 and 75 wt.% Na_2SO_4 + 25 wt.% NaCl salts. The presence of preformed Al_2O_3 scale reduced the consumption rate of aluminum by delaying the formation of internal oxides and sulfides and leading to the formation of denser and more adherent Al_2O_3 scale.

(3) The presence of chloride in the mixed salts accelerated the corrosion extent of as-sprayed and pre-oxidized coating, which can be attributed to the self-sustainable characteristic of repeated oxidation and chlorination of beneficial Al.

Acknowledgments

This research was financially supported by foreign scientific and technological cooperation project of Jiangxi province (20151BDH80002) and International S&T Cooperation Program of China (2013DFR50900).

References

1. N. Eliaz, G. Shemesh, and R.M. Latanision, Hot Corrosion in Gas Turbine Components, *Eng. Fail. Anal.*, 2002, **9**, p 31-43
2. A. Rabiei and A.G. Evans, Failure Mechanisms Associated with the Thermally Grown Oxide in Plasma-sprayed Thermal Barrier Coating, *Acta Mater.*, 2000, **480**, p 3963-3976
3. N.P. Padture, M. Gell, and E.H. Jordan, Thermal Barrier Coatings for Gas-turbine Engine Applications, *Science*, 2002, **296**, p 280-284
4. J.R. Nicholls, Advance in Coating Design for High-performance Gas Turbines, *MRS. Bull.*, 2003, **28**, p 1-14
5. M.P. Brady, B. Gleeson, and I.G. Wright, Alloy Design Strategies for Promoting Protective Oxide-scale Formation, *J. Met.*, 2000, **52**, p 16-21
6. W.R. Chen, R. Archer, X. Huang, and B.R. Marple, TGO Growth and Crack Propagation in a Thermal Barrier Coating, *J. Therm. Spray Technol.*, 2008, **17**, p 858-864
7. Z.B. Bao, Q.M. Wang, W.Z. Li, J. Gong, T.Y. Xiong, and C. Sun, Corrosion Behaviour of AIP NiCoCrAlYSiB Coating in Salt Spray Tests, *Corros. Sci.*, 2008, **50**, p 847-855
8. H. Assadi, F. Gartner, T. Stoltenhoff, and H. Kreye, Bonding Mechanism in Cold Gas Spraying, *Acta Mater.*, 2003, **51**, p p4379-4394
9. T. Stoltenhoff, H. Kreye, and H.J. Richter, An Analysis of the Cold Spray Process and Its Coatings, *J. Therm. Spray Technol.*, 2002, **11**, p 542-550
10. P. Richer, M. Yandouzi, L. Beauvais, and B. Jodoin, Oxidation Behaviour of CoNiCrAlY Bond Coats Produced by Plasma, HVOF and Cold Gas Dynamic Spraying, *Surf. Coat. Technol.*, 2010, **204**, p 3962-3974
11. W.R. Chen, E. Irissou, X. Wu, J.G. Legoux, and B.R. Marple, The Oxidation Behaviour of TBC with Cold Spray CoNiCrAlY Bond Coat, *J. Therm. Spray Technol.*, 2011, **20**, p p132-138
12. Q. Zhang, C.J. Li, C.X. Li, G.J. Yang, and S.C. Liu, Study of Oxidation Behavior of Nanostructured NiCrAlY Bond Coatings Deposited by Cold Spraying, *Surf. Coat. Technol.*, 2008, **202**, p p3378-3384
13. L. Ajdelsztajn, B. Jodoin, G.E. Kim, J.M. Schoenung, and J. Mondoux, Cold Spray Deposition of Nanocrystalline Aluminum Alloys, *Metall. Mater. Trans. A*, 2005, **36**, p 657-666
14. P. Richer, A. Zúñiga, M. Yandouzi, and B. Jodoin, CoNiCrAlY Microstructural Changes Induced during Cold Gas Dynamic Spraying, *Surf. Coat. Technol.*, 2008, **203**, p 364-371
15. J.A. Goebei and F.S. Pettit, Na_2SO_4-Induced Accelerated Oxidation (Hot Corrosion) of Nickel, *Metall. Trans.*, 1970, **1**, p p1943-1954
16. R.A. Rapp, Hot Corrosion of Materials: A Fluxing Mechanism?, *Corros. Sci.*, 2002, **44**, p 209-221
17. N. Otsuka and R.A. Rapp, Hot Corrosion of Preoxidized Ni by a Thin Fused Na2SO4 Film at 900 °C, *J. Electrochem. Soc.*, 1990, **137**, p 46-52
18. N. Birks and G.H. Meier, *Introduction to High Temperature Oxidation of Metals*, 2nd ed., Cambridge University Press, London, 2006
19. R.A. Rapp and Y.S. Zhang, Hot Corrosion of Materials: Fundamental Studies, *JOM*, 1994, **46**, p 47-55
20. P.D. Jose, D.K. Gupta, and R.A. Rapp, Solubility of α-Al_2O_3 in Fused Na_2SO_4 at 1200 K, *J. Electrochem. Soc.*, 1985, **3**, p 735-737
21. M.K. Hossain and S.R.J. Saunders, A Microstructural Study of the Influence of NaCl Vapor on the Oxidation of a Ni-Cr-Al Alloy at 850 °C, *Oxid. Met.*, 1978, **12**, p 1-22
22. N. Hiramatsu, Y. Uematsu, T. Tanaka, and M. Kinugasa, Effect of Alloy Elements on NaCl-induced Hot Corrosion of Stainless Steels, *Mater. Sci. Eng. A*, 1989, **120**, p 319-328
23. Y. Liang and Y. Che, *Codata Key Values for Thermodynamics*, Northeastern University Press, Lebanon, 1993 (**in Chinese**)
24. C. Zhou, R. Cai, S.K. Gong, and H. Xu, Hot Corrosion of Al-CuFeCr Quasicrystalline Coating on Titanium Alloys with NaCl Deposit, *Surf. Coat. Technol.*, 2006, **201**, p 1718-1723